

PAPER • OPEN ACCESS

Observation of thermally-induced magnetic relaxation in a magnetite grain using off-axis electron holography

To cite this article: Trevor P. Almeida *et al* 2017 *J. Phys.: Conf. Ser.* **902** 012001

View the [article online](#) for updates and enhancements.

Related content

- [Hydrothermal synthesis, off-axis electron holography and magnetic properties of Fe₃O₄ nanoparticles](#)
Trevor P Almeida, Adrian R Muxworthy, Wyn Williams *et al.*
- [Study of grain morphology of various magnetite samples by means of EBSD](#)
A Koblischka-Veneva and M R Koblischka
- [Visualisation of high temperature magnetisation states in magnetite grains using off-axis electron holography](#)
T P Almeida, A R Muxworthy, A Kovács *et al.*

Observation of thermally-induced magnetic relaxation in a magnetite grain using off-axis electron holography

Trevor P. Almeida^{1*}, Adrian R. Muxworthy², András Kovács³, Wyn Williams⁴ and Rafal E. Dunin-Borkowski³

¹School of Physics and Astronomy, University of Glasgow, Glasgow, G12 8QQ, UK.

²Department of Earth Science and Engineering, South Kensington Campus, Imperial College London, London, SW7 2AZ, UK.

³Ernst Ruska-Centre for Microscopy and Spectroscopy with Electrons (ER-C) and Peter Grünberg Institute, Forschungszentrum Jülich, D-52425 Jülich, Germany.

⁴School of GeoSciences, University of Edinburgh, Edinburgh, EH9 3JW, UK.

Abstract. A synthetic basalt comprising magnetic Fe₃O₄ grains (~ 50 nm to ~ 500 nm in diameter) is investigated using a range of complementary nano-characterisation techniques. Off-axis electron holography combined with *in situ* heating allowed for the visualisation of the thermally-induced magnetic relaxation of an Fe₃O₄ grain (~ 300 nm) from an irregular domain state into a vortex state at 550°C, just below its Curie temperature, with the magnetic intensity of the vortex increasing on cooling.

1. Introduction

Palaeomagnetists study the magnetic signal recorded by magnetic minerals within rocks to understand a wide range of geological problems, e.g., plate tectonic movements and geomagnetic field variation. Small, magnetically-uniform grains, termed single domain (SD), are considered the strongest remanence carriers with good stability over geological time periods [1]. However, the magnetic signature in most rocks is usually dominated by larger magnetic grains (~ 0.1 to 10 µm) that display non-uniform magnetic structures, i.e., single or multiple vortices, that are commonly referred to as pseudo-SD (PSD) particles. Magnetite (Fe₃O₄) is usually considered the most important magnetic mineral due to its high abundance and spontaneous magnetization. In igneous rocks, the leading source of magnetic induction is thermal remanent magnetization (TRM), which is acquired in the direction of the ambient geomagnetic field as the grains cool below their Curie temperature (T_C (~ 580°C for Fe₃O₄)). However, current understanding of the thermomagnetic behaviour of PSD remanence is restricted to bulk magnetic measurements and numerical models. Hence, our knowledge of PSD remanence and magnetic stability as a function of temperature is poor, and understanding of reliability of most Earth and planetary paleomagnetic signals is limited.

The transmission electron microscopy (TEM) technique of off-axis electron holography allows for the nano-scale imaging and quantitative measurements of magnetic induction within and around materials as a function of temperature [2]. Recent studies have shown that PSD vortex states in synthetic Fe₃O₄ powdered grains are generally stable as they approach the T_C and recover their signal on cooling [3-5]. However, few studies have shown visually the thermoremanent behaviour of PSD Fe₃O₄ grains dispersed within a matrix, which are more representative of rocks. In this context, a synthetic basalt containing nano-scale Fe₃O₄ grains is investigated using a range of nano-characterisation techniques, and off-axis electron holography is combined with the heating of PSD magnetite (Fe₃O₄) grains *in situ* within the TEM.

*Author to whom correspondence should be addressed: trevor.almeida@glasgow.ac.uk.



2. Experimental

The synthetic basalt was produced via a glass-ceramic method by heating laboratory grade powders in a vertical temperature-controlled tube furnace under an oxygen partial pressure at 1400°C, before quenching and reheating at 750°C, as described previously [6]. The sample was mounted in epoxy resin and polished for secondary electron microscopy (SEM) using an FEI Quanta 200 ESEM FEG, whilst their elemental constituents were identified by energy dispersive X-ray (EDX) analysis. Conventional bright-field (BF) imaging was performed using a FEI Tecnai TEM operated at 200 kV. For structural characterisation, part of the synthetic basalt was crushed into a fine powder and deposited onto silicon substrates for crystallographic identification using X-ray diffractometry (XRD) (PANalytical X'Pert Pro Diffractometer). Magnetic measurements were conducted at Imperial College London and the Institute for Rock Magnetism, University of Minnesota. The first-order reversal curve (FORC) and high temperature thermomagnetic curves were measured using a Princeton Measurements Vibrating Sample Magnetometer (VSM) fitted with a furnace; heating was performed in flowing He. Low-temperature hysteresis measurements were made from 15 to 295 K (in 10 K intervals) using a helium-cooled Princeton Measurements VSM.

For *in situ* heating TEM investigations, desirable regions were deposited and welded with platinum to contacts on a DENSSolutions® double-tilt MEMS-based heating chip in a focused ion beam SEM before being milled into thin sections. Off-axis electron holograms were acquired at 300 kV in Lorentz mode in a Titan 80-300 TEM (ER-C) [8] with a charge-coupled device camera and an electron biprism, operated at 90 V. The directions of magnetization in the Fe₃O₄ particle were reversed initially at 20°C by tilting the sample ± 75° and turning on the objective lens to apply a magnetic field of > 1.5 T. The objective lens was then turned off, and the sample tilted back to 0° for hologram acquisition under field-free conditions with the particle magnetized in opposite directions, and the mean inner potential (MIP) was then separated from the magnetic potential [2-5]. Electron holograms were then acquired under field-free conditions (residual field < 0.2 mT) during *in situ* heating at 400°C, 500°C and 550°C, and again upon cooling. The heating experiment was then repeated, and magnetization reversal was performed by turning on the objective lens at ± 75° at each temperature interval to obtain the MIP, which was then subtracted from the total phase shift attained during the first heating stage to isolate the Fe₃O₄ particle's true remanent magnetisation [4, 5].

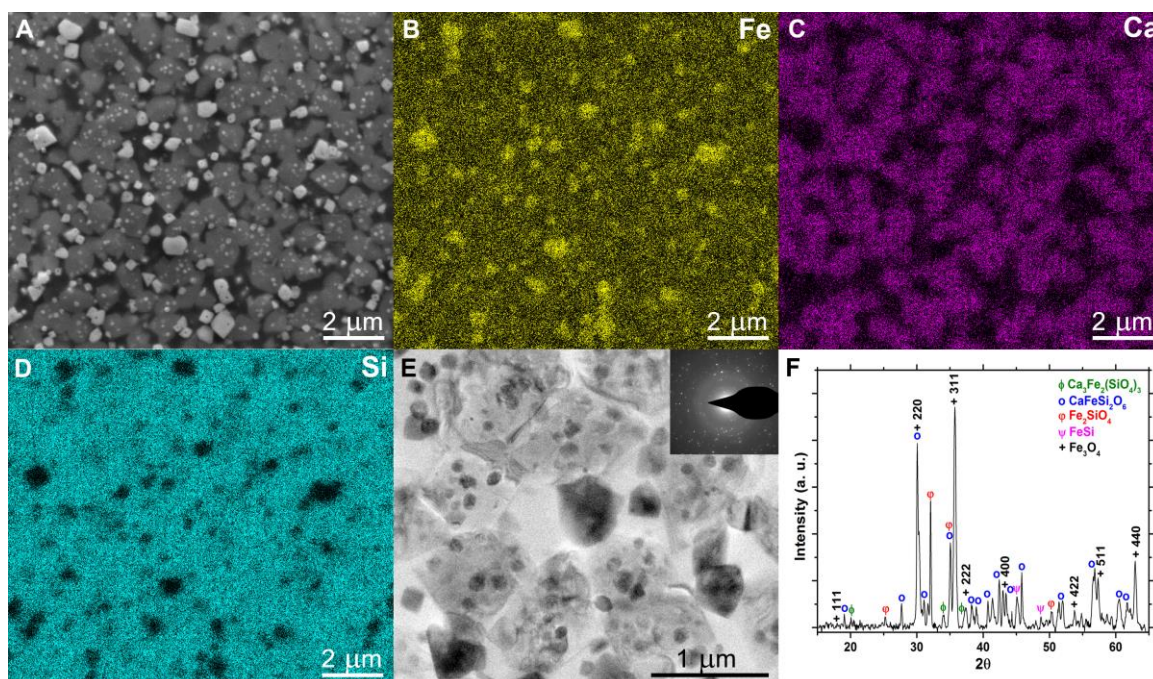


Figure 1. (A) BSE SEM image of the synthetic basalt; and (B-D) associated EDX chemical maps showing the elemental distribution of (B) iron; (C) calcium; and (D) silicon. (E) BF TEM image of the Fe₃O₄ grains within the silicate matrix ranging from ~ 50 to ~ 500 nm, with SAED (inset). (F) XRD pattern of the synthetic basalt, confirming the Fe₃O₄ phase (indexed, JCPDS 75-449), as well as the additional phases of CaFeSi₂O₆, Ca₃Fe₂(SiO₄)₆ and FeSi.

3. Results

The furnace annealing of the precursor powder mixture led to the production of a synthetic basalt comprising Fe_3O_4 grains of varied size, morphology and magnetic properties, the evidence for which is now presented in detail.

Fig. 1 provides information on the chemical distribution, morphology, size and structure of the synthesised sample. The backscattered-electron (BSE) SEM image and corresponding EDX maps of Fig. 1A-D present the elemental distribution within the sample. Comparison of the BSE image (Fig. 1A) with the Fe chemical map (Fig. 1B) confirm the bright regions in the BSE image are Fe-rich, and hence attributed as the Fe_3O_4 particles. Some areas are observed to be high in Ca content (Fig. 2C), whilst the remaining area is shown to be Si-rich (Fig. 1D). The BF TEM image of Fig. 1E displays Fe_3O_4 grains ranging in size, from ~ 50 nm to ~ 500 nm, along with the surrounding glass ceramic matrix. It is evident that the smaller Fe_3O_4 grains are generally confined within glassy regions, separate from the larger Fe_3O_4 grains. The peaks in the XRD pattern of Fig. 1F are in good agreement with the presence of Fe_3O_4 (Joint Committee on Powder Diffraction Standards (JCPDS) ref: 75-449), as well as pyroxene hedenbergite ($\text{CaFeSi}_2\text{O}_6$, JCPDS 70-1876), andradite ($\text{Ca}_3\text{Fe}_2(\text{SiO}_4)_3$, JCPDS 84-1938), FeSi (JCPDS 86-0795) and Fayalite (Fe_2SiO_4 , JCPDS 71-1673).

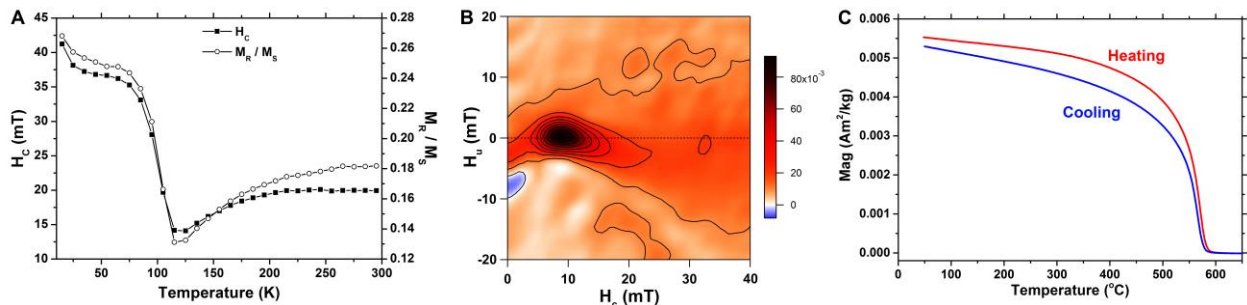


Figure 2. (A) Graph of coercive force and M_{rs}/M_s as a function of temperature (15 K to 295 K). (B) FORC diagram acquired at room temperature (smoothing factor = 7). The measurement time was 250 ms. (C) Thermomagnetic curves of the synthetic basalt. Heating was performed in flowing helium, in a field of 300 mT.

The hysteresis parameters H_c and M_{rs}/M_s are plotted as a function of temperature (15 K to 295 K) in Fig. 2A and displays behaviour typical of Fe_3O_4 , with the Verwey transition at ~ 120 K. The FORC diagram of Fig. 2B shows the sample to exhibit behaviour characteristic of a mixture of SD and PSD grains, whereby the negative region close to the vertical H_u -axis indicates that the controlling anisotropy in SD grains is uniaxial, whilst the curvature along the H_c -axis reveals the presence of PSD grains. High-temperature thermomagnetic analysis (Fig. 2C) indicates that the Fe_3O_4 NPs within the synthetic basalt are thermally stable. The T_C was determined from the heating curve using the second-derivative method [8] and calculated as $585 \pm 5^{\circ}\text{C}$, which is in good agreement with stoichiometric Fe_3O_4 .

Fig. 3 presents the thermomagnetic behaviour of an individual Fe_3O_4 grain embedded in the silicate matrix as it is heated from 20°C to 550°C and then cooled back to 20°C . The BF TEM image of Fig. 3A displays the square Fe_3O_4 grain with sides ~ 300 nm in length and a hole located in its centre, with the associated selected area electron diffraction (SAED) pattern (inset). Fig. 3B displays a magnetic induction map of this Fe_3O_4 grain at 20°C after saturation, and reveals its magnetization to resemble a horseshoe-like shape, with the magnetic contours flowing in a clockwise direction, along with a component of stray magnetic field, indicative of a PSD state. An increase in temperature to 400°C (Fig. 3C) results in a slight widening of the contours and further broadening is evident in Fig. 3D, recorded at 500°C . At 550°C , the magnetization closes in to a vortex structure (Fig. 3E), the intensity of which becomes more prominent upon cooling to 500°C (Fig. 3F). The magnetic contours of the vortex are observed to narrow and the vortex magnetization intensity to increase further upon cooling back to 20°C (Fig. 3G & 3H). As a consequence of the vortex closure, it is evident that the stray magnetic field (Fig. 3H) has become notably less pronounced than observed prior to heating (Fig. 3B), i.e., it has partially demagnetised.

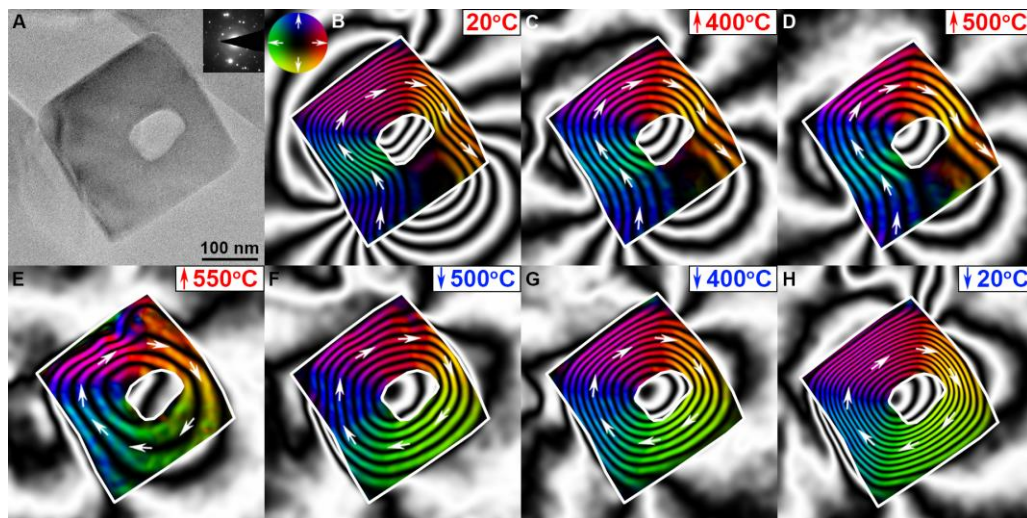


Figure 3. (A) BF TEM image of a square Fe_3O_4 grain within the silicate matrix (~ 300 nm along each side), exhibiting a hole at its centre, with associated SAED pattern (inset). (B-H) Magnetic induction maps reconstructed from holograms taken at (B) room temperature (20°C); and during *in situ* heating to (C) 400°C ; (D) 500°C ; and (E) 550°C ; as well as upon subsequent cooling to (F) 500°C ; (G) 400°C ; and (H) 20°C . The contour spacing is 0.39 radians for all magnetic induction maps and direction is shown using arrows, as depicted in the colour wheel.

4. Discussion

This combined SEM, TEM, XRD and magnetic investigation of the synthetic basalt has provided evidence for the growth of Fe_3O_4 grains, ranging from ~ 50 to ~ 500 nm in size, within the silicate matrix. The smaller 50 nm grains are confined within Ca-rich glassy regions, and hence considered as hedenbergite regions; these SD domain grains are considered to form during the rapid quenching stage of synthesis [6]. The larger grains, ~ 500 nm in diameter, are likely to contribute the PSD signal in the FORC diagram. Complementary to the presence of the Verwey transition in the Fig 2A, the thermomagnetic curve displays a T_C characteristic of stoichiometric Fe_3O_4 , and shows a significant drop in magnetisation above 400°C , providing a suitable temperature range for investigating the magnetic relaxation of PSD Fe_3O_4 grains using electron holography.

The Fe_3O_4 grain in Fig. 3 exhibits a horseshoe-like magnetisation state (Fig. 3B) that reduces in intensity upon heating to 400°C and 500°C , closing into a vortex structure at 550°C , which then steadily increases in intensity upon cooling, with its stray magnetic field intensity reducing significantly compared to its initial state. It is apparent that the thermal energy imparted on the Fe_3O_4 grain at 550°C has promoted the transition to a more energetically-favourable vortex state. For bulk samples, the measurable net directional and intensity information is acquired from the stray magnetic fields of the grains and it is evident this signal is reduced after vortex closure, losing both its original directional and intensity information. Hence, whilst the domain structure remains relatively stable during heating, at close to the T_C ($> 500^\circ\text{C}$) the original palaeomagnetic signal can be lost due to thermal relaxation.

In summary, complementary nano-characterisation techniques have confirmed the synthesis of SD and PSD Fe_3O_4 grains within a synthetic basalt. Electron holography combined with *in situ* heating allowed for the visualisation of the magnetic relaxation of an PSD Fe_3O_4 grain into a vortex structure just below the T_C .

References

- [1] Néel L 1995 *Adv. Phys.* **4**, 191-242 L.
- [2] Dunin-Borkowski R E *et al* 1998 *Science* **282**, 1868-1870.
- [3] Almeida T P *et al* 2014 *Geophys. Res. Lett.*, **41**, 7041–7047.
- [4] Almeida T P *et al* 2016 *Sci. Adv.*, **2**, e1501801.
- [5] Almeida T P *et al* 2016 *Geophys. Res. Lett.*, **43**, 8426-8434.
- [6] Almeida T P *et al* 2014 *Geochem. Geophys. Geosyst.*, **15**, 161–175.
- [7] Boothroyd C, Kovács A and Tillmann K 2016 *JLSRF* **2**, A44.
- [8] Tauxe L 1998 *Paleomagnetic Principles and Practice*, (Kluwer Acad., Dordrecht, Netherlands).

Acknowledgements

The authors would like to thank NERC (grant NE/J020966/1) and ERC (grant 320832) for funding.